Effect of brazing temperature on microstructure and mechanical properties of TiAl/ZrB_2 joint brazed with CuTiZrNi filler

Gang Wang[1,*], Yunlong Yang[1], Peng Wu[1], Da Shu[1*], Dongdong Zhu[2], Caiwang Tan[3], Wei Cao[4,1]

1 School of Mechanical and Automotive Engineering, Anhui Polytechnic University, Wuhu 241000, China

2 Key Laboratory of Air-Dirven Equipment Technology of Zhejiang Province, Quzhou University, Quzhou 324000, China

3 State Key Laboratory of Advanced Welding and Joining, Harbin Institute of Technology, Harbin 150001, China

4 Nano and Molecular Systems Research Unit, University of Oulu, P.O. Box 3000, Oulu, 90014, Finland

[*]Corresponding author.

E-mail addresses: gangwang@ahpu.edu.cn (G. Wang), sd@ahpu.edu.cn (D. Shu).

Abstract

The TiAl alloy and ZrB_2-SiC ceramic are promising materials used at high temperatures. One route to extend their unique applications under extreme conditions relies on successful brazing them together with proper fillers. In this work, brazing temperature influences on microstructural, mechanical, and fractural properties were systemically studied for brazed joints after brazing the TiAl to the ZrB_2-SiC with amorphous CuTiZrNi fillers. An optimized brazing was found at 1183 K for 1200 s, yielding a high shear strength of 187 MPa. The joints were mainly consisted of AlCuTi, Ti_2Al, $(Ti,Zr)_2(Cu,Ni)$, TiB,TiB_2, TiCu Ti_5Si_3, and TiC phases. Brazing temperature substantially changed joint composites. It is found that lower temperature lead to insufficient reaction and remained filler and higher ones to large stress-induced microcracks. Based on element diffusion, a formation mechanism of brazed joint was also proposed.

Keywords: Brazing; Amorphous filler; Microstructure; Shear strength

Introduction

As promising substitutes to nickel alloys, the TiAl alloys are endowed with specifically high strength, excellent mechanical behaviors, and durable creep and corrosion resistance at high temperatures [1-3]. Joining the TiAl alloys to other high temperature materials, e.g. ceramics, become necessary and attractive to extend alloy applications. The yielded metal-ceramic complexed are endowed with advantage properties of both joint counterparts.

So far, the TiAl alloys have been welded via several methods, such as fusion joining [4, 5], diffusion bonding [6-8] and brazing [9-12]. Among them, brazing is considered as an effective and superior method thanks to its convenience, low cost and high-quality brazed joints in the metal-ceramic connection technologies. The AgCu eutectic alloy was employed in the brazing of the metalized porous Si_3N_4 ceramic to the TiAl alloy. Significant improvements of the mechanical properties were reached for the Si_3N_4/TiAl joint were reached due to the laser-induced metallization process [13]. Yang *et al*. reported a joining of the TiAl alloy to Al_2O_3 ceramic with a W-doped AgCuTi alloy filler. The addition of W particles on the filler could releases residual stress formation during cooling [14]. The weldability of Ti6Al4V/ZrO_2 joints was studied by using the Ag-Cu metallic filler, and a high shear strength of 52 MPa was yielded [15]. Furthermore, in order to get sound joints, some amorphous filler are also used to braze metals-ceramic. Li *et al* brazed a TiAl alloy with amorphous and crystalline TiZrCuNiCoMo filler alloys. Compared with crystalline counterparts, the amorphous alloys brought better brazeability on the surface of the Ti-47Al-2Nb-2Cr-0.15B alloy, and higher tensile strengths of the joints

[16]. Cao *et al* used NiCrSiB amorphous filler foils to braze Ti alloy and ZrO_2 ceramic. A high value of 284.6 MPa shear strength was obtained [17].

As joining candidates to the TiAl side, ZrB_2-SiC (ZS) ceramics are well-known for their high temperature structural applications in aerospace and spacecraft components. This stems from the featured materials properties of excellent oxidation and thermal shock resistances, superior chemical stabilities in addition to the high melting temperatures [18,19]. The brazeability of these ceramics with themselves, metals or other materials has been reported during the last decades [20-25]. Valenza *et al*. formed Ti6Al4V/ZrB_2-SiC joints with a composite filler consisted of an Ag-based alloy with the Cu interlayer. The addition of cooper contributed to formations of intermetallic compounds which improves the joint strength [20]. Besides the Cu fillers, the Ni powders were also employed to braze the ZS and lead to a maximum shear strength of 60 MPa at the joint [23]. Wang *et al*. loaded the TiCuZrNi fillers on the Cu foam in brazing and obtained an optimum shear strength of 435 MPa at the joint [26]. The above analysis shows that the Ag-, Cu-, Ti- and Ni-based fillers benefit the overall strength of the joints when brazing ZS alloys.

In this work, TiAl alloy and ZS ceramic were brazed with amorphous CuTiZrNi fillers at different temperatures. Influences of brazing temperature on microstructure and mechanical properties of the TiAl/ZS joint were systematically investigated. Besides identifying an optimized brazing temperature, the formation mechanism was proposed based on element diffusion schemes.

Experimental

Prepared via arc melting, the TiAl alloy used in the present work has a formula of

Ti-48Al-2Nb-2Cr alloy (at. %). The high purity Ti, Al, Cr metals, and an Nb-Al intermediate alloy were employed as precursors. The detailed preparation process and microstructure were reported in a previous work [27]. The ZrB_2 (80 vol%) and SiC(20 vol %) powder mixtures were hot pressed at 2223 K for 3600 s under vacuum and a pressure of 30 MPa. The single roller-spinning technique was used to prepare the $Cu_{41.83}Ti_{30.21}Zr_{19.76}Ni_{8.19}$ (at. %) amorphous filler. It has a thickness of 30 μm, and well characterized structures [28].

The raw Ti-48Al-2Nb-2Cr alloy and ZS were cut into 4 mm × 4 mm × 4 mm and 10 mm × 10 mm × 4 mm for microstructure observation and shear strength testing. Surfaces of the TiAl alloy and ZS ceramic were carefully polished beforehand, and then ultrasonically cleaned for 600 s. Parts to be brazed were heated up to designed temperatures at +0.167 K/s. The brazings were performed at 1153 K, 1183 K, 1213 K and 1243 K for 1200 s, respectively. After brazing, samples were first cooled at a rate of -0.083 K/s to reach 573 K, and then cooled in the furnace. The whole brazing process was carried out under vacuum with pressure $< 1 \times 10^{-3}$ Pa.

The samples were characterized via scanning electron microscopy (SEM) on a SU-8010 SEM. It is equipped with energy-dispersive X-ray spectrometer (EDS) for element quantifications. An X-ray diffractometer (XRD, Bede D1) and a transmission electron microscope (TEM, Tecnai G2 F30) were employed for microstructural and microscopic determinations. For the XRD analysis of phase in the brazed joints, the method of ‘layer-by-layer polishing’ was used. Shear strength testing was performed using an Instron 5500 testing machine. An average value was obtained from three

samples for each brazing parameter.

Results and discussion

Fig.1 depicts the microstructures and corresponding EDS results from the joint of the ZS/TC4 brazed at 1213 K for 1200 s. ZS ceramic and TiAl alloy are well bonded, and obvious reaction layers are detected in both ZS ceramic and TiAl alloy interfaces, as indicated in Fig.1a. Element distributions in the brazed joint are shown in Fig.1b to Fig.1i. The Ti, Cu, Zr and Ni are well identified at the brazed joint (Fig.1b, and Fig.1d to Fig.1f), but the Al element is mainly found at the TiAl alloy side of the brazed joint, as shown in Fig. 1c. B, C, and the Si at the ZS ceramic side after migration from the ZS ceramic, as shown in Figs. 1g, 1h and 1i. From the above results, it is proved that the strong atomic diffusion occurred in the brazed joint.

A typical joint microstructure is shown for the ZS/CuTiZrNi/TiAl brazed at 1213 K for 1200 s in Fig.2A. A defect-free brazed joint with 40 μm width was obtained. In the figure, zone I and III respectively stand for reaction layers formed at ZS and TC4 sides. The average width of zone I is about 10 μm. Zone II was the center zone of the joint. Figures 2b and 2c are the zoomed images of zones I and III. Based on contrast, zone I mainly consists of two lamellar-like phases, marked by A and B. Zone II is a region mixed by three phases, as marked by C, D and E. For zone III, there are many needle-like phases, marked as F. Table 1 tabulates chemical compositions of phases A-H in the brazed joint.

We analyzed the element distributions according to the EDS results. The Al, Cu, and Ti stay in the gray phase (A) with an approximate ratio of 1:1:1. According to the

Al-Cu-Ti ternary alloy phase diagram, a boundary curve exists between the AlCuTi and TiAl. As a result, the AlCuTi can be directly contiguous to the TiAl phase of the base material [29]. Moreover, the AlCuTi phase was also found at the brazed joints of Al_2O_3/AgCuTi/ TiAl alloy and TiAl/BAg-8/TiAl alloy [30]. Following the result, spot A is assigned to the AlCuTi. Similarly, the main elements in the black phase B are Ti and Al with an approximate ratio of 2:1, and thus compose the Ti_2Al phase. The Ti_2Al also acts an intermediate phase during the phase transformation between the Ti_3Al and TiAl phases [31, 32]. Besides, a reaction of Ti + TiAl $\rightarrow Ti_2Al$ can also lead to the Ti_2Al formation during the hot press sintering [33]. The Zr, Ti, Cu, and Ni are the main elements at the spot C in zone II. A careful look at the element abundance shows that the Cu + Ni is around 1/2 compared to the Ti + Zr. Indeed, the element paris of Ti+Zr and Cu+Ni are chemically compatible, and physically soluble to each other. Consequentially, the $(Ti,Zr)_2(Cu,Ni)$ is formed and can be considered as a generalized phase of Ti_2Cu, Zr_2Cu, Ti_2Ni and Zr_2Ni. This claim is supported by previous works [34-37]. The black spot D is mainly formed by the B and Ti, and ascribed to a mixture of TiB and TiB_2 subjected to reactions of $Ti+ZrB_2 \rightarrow TiB_2+Zr$ and $Ti+TiB_2 \rightarrow TiB$. For spot E, it is mainly composed of Ti and Cu at an approximate ratio of 1:1. According to the Ti-Cu binary diagram, spot E is consider as TiCu phase, as a result from an eutectic reaction of $L \rightarrow TiCu + Ti_2Cu$. Spot F is mainly consisted of Si, C and Ti elements. The amount of Si is consistent with the result from Fig.1h. During the brazing process, Ti easily reacts with SiC, resulting in the formation of Ti_5Si_3 and TiC phases ($Ti + SiC \rightarrow Ti_5Si_3 + TiC$). The element analysis through EDS agrees with the

XRD result as shown in Figure 3 for the sample brazed at 1213 K for 1200 s. All proposed phases are well indexed in the XRD patterns. Based on the aforementioned results in Table 1, XRD and phase diagrams, the AlCuTi, Ti_2Al, $(Ti,Zr)_2(Cu,Ni)$, $TiB+TiB_2$, TiCu and Ti_5Si_3+TiC are assigned to phases A-F.

Table 1 Chemical composition and possible phase of each spot marked in Figure 2 (at. %)

Position	Elements										Possible phase
	Ti	Zr	Cu	Ni	Al	B	Si	Nb	Cr	C	
A	38.50	0.58	25.30	3.84	30.50	-	-	0.51	0.77	-	AlCuTi
B	60.30	3.39	1.49	3.47	29.20	-	-	1.19	0.95	-	Ti_2Al
C	41.10	8.60	15.90	8.09	11.72	3.05	0.92	1.76	1.50	7.36	$(Ti,Zr)_2(Cu,Ni)$
D	50.30	1.74	1.10	0.28	1.61	36.80	0.07	-	-	8.10	$TiB+TiB_2$
E	26.10	8.67	30.10	4.63	10.50	4.20	0.56	1.23	0.94	13.07	TiCu
F	29.11	14.93	9.30	2.55	1.94	11.0	19.52	-	-	11.65	Ti_5Si_3+TiC

From the above analysis, the TiAl/ZS brazed joint undergoes a formation mechanism which is visualized in Fig.4 and explicated as follows.

1) During the heat process, firstly, the filler was plastically deformed and tightly contact with the TiAl alloy and ZS ceramics, as shown in Fig. 4a. At a higher temperature above the filler's melting point, the surface of the base materials was wetted by the molten filler. Meanwhile, the bases were also partially dissolved into the molten alloy. Main elements (Ti, Al, Cu, Zr, Ni, B, C and Si) started to diffuse, as shown in Fig. 4b.

2) Continuous increases of brazing temperature gradually ruin the γ-TiAl and α_2-Ti_3Al phases in the Ti-48Al-2Nb-2Cr base materials by decreasing the Ti and Al contents due to element diffusion. And the contents eventually fell below the formation threshold [38]. Chemical reactions turned out as $TiAl \rightarrow Al + Ti_2Al$ and $Ti_3Al \rightarrow Ti +$

Ti_2Al. Thus, the Ti_2Al was formed. For ZS ceramic side, a reaction of Ti + SiC → Ti_5Si_3 + TiC occurred as a result of Ti's strong affinities to Si and its lowest Gibbs free energy among the wielding peers [39]. Compared to other Ti-Cu products, the TiCu owns the lowest Gibbs free energy [40] and can be formed via the reaction Ti + Cu → TiCu in the middle of joint. Meanwhile, an eutectic reaction L → Ti + $(Ti,Zr)_2(Cu,Ni)$ took place following the Cu-Ni-Ti(Zr) ternary phase diagram analysis, as shown in Fig. 4c.

3) When the temperature further increased to the brazing temperature and holding, AlCuTi phase appeared by the reaction L + TiAl + Ti_3Al→AlCuTi in TiAl alloy side [41]. For ZS ceramic side, the Ti could react with the B. It exists both at the filler and TiAl alloy sides. The TiB and TiB_2 can be yielded from Ti + B → TiB_2 and Ti + TiB_2→ TiB. At the same time, $(Ti,Zr)_2(Cu, Ni)$, TiCu, Ti_5Si_3 and TiC phases grew and aggregated together (see Fig. 4d).

4) At the cooling stage, more and more $(Ti,Zr)_2(Cu, Ni)$ phase was formed due to the reaction of β-Ti→ α-Ti + $(Ti,Zr)_2(Cu, Ni)$. However, α-Ti and β-Ti were not detected, which is different from the previous report [24, 27]. The interfacial reaction layer contains AlCuTi and Ti_2Al. its thickness increased at the TiAl alloy side, as shown in Fig. 4e.

Figure 5 shows the shear strength of TiAl/ZS brazed joint for 1200 s at different brazing temperature. A rather small shear strength of 45 MPa was yielded at 1153 K. This is mainly caused by the insufficient atomic diffusion and reaction between base alloy and filler metal. At a 1183 K brazing temperature, the strength reached the peak

value of 187 MPa. At 1213 K, the shear strength was 177 MPa, a slightly lower than the maximum value. At a1243 K of the brazing temperature, the resulted shear strength dropped to 125 MPa.

The temperature dependent brazing results were further studied. Figure 6 demonstrates the microstructure of TiAl/ZS brazed joint at different brazing temperature for 1200 s. Overall, three characteristic zones, which is similar for the condition of 1213 K for 1200 s, can be obviously found in all joints obtained by different brazing temperature, as shown in Figs.6a, 6d, 6g and 6j. However, certain changes turn out at each zone following the temperature increase. In the middle of joints, the amount and size of TiCu, TiB and TiB_2 phases increased with the brazing temperature. It is worth noting that some white block phases were formed at 1153 K and 1183 K. Moreover, the size and amount of white block phases drastically decreased, as shown in Figs. 6c and 6f. The chemical composition of white phases was detected, as shown in Table 2. The results indicated that the chemical composition of white phases is similar to the original filler, especially the Ti, Cu, Zr and Ni elements. It is reported that the melting point of $Cu_{41.83}Ti_{30.21}Zr_{19.76}Ni_{8.19}$ filler is 1133 K, slightly lower than the brazing temperature of 1153 K [42]. Thus, the white block phase is inferred as residual filler due to inadequate dissolution and element diffusions from the filler. Theses insufficient behaviors are not conducive to the joint strength, leading to the minimum value of shear strength, as shown in Fig.1. The thickness of reaction layer in TiAl alloy side increased from 5 μm to 10 μm. The quantity of the Ti_2Al phase increased with the brazing temperature while the AlCuTi

phase decreased, as shown in Figs.6b, 6e, 6h and 6k. Due to the limited solubility of Cu in the TiAl alloy [43] and the formation of continuous layer of Ti_2Al phase, the atomic diffusion between TiAl alloy and filler can be hindered, leading to the slow growth of AlCuTi phase at the TiAl side. Some micro-cracks were observed in the brazed joint at 1243 K, as shown in Fig.6k. The formation of micro-cracks can be explained as follows. During the cooling process, yielded residual stresses turned out in the brazed joint because of thermal expansion coefficient mismatches and Young's modulus differences between the TiAl alloy and the filler. The existence of these micro-cracks is harmful to the mechanical properties of joint, resulting in the decrease of shear strength, as shown in Fig.1. In ZS side, the amount and size of Ti_5Si_3 and TiC increased with the brazing temperature, as shown in Figs. 6c, 6f, 6i and 6l. Reaction layer became thicker, from 2 μm to 10 μm. From the results of Fig.1, good joints were obtained at 1183 K and 1213 K. The phenomenon can be deduced from the microstructural analysis as follows. In general, an optimized thickness is normally required for the reaction layer at the brazed joints. The thickness is regulated by brazing parameters [44]. The thickness of reaction layer affects the shear strength of joints. Under a lower brazing temperature, a smaller quantity of diffused atoms leads to insufficient reaction but filler residuals between the filler and base materials, as shown in Figs.6a, 6b and 6c. At a higher brazing temperature, a larger amount of diffused atoms lead to formation of thicker reaction layers. The thicker reaction layers yielded residual stress in the joint, and lead to the formation of micro-crack, as shown in Figs.6j and 6k. In addition, the intrinsic brittleness of Ti_5Si_3 and TiC in the layers

deteriorates mechanical properties of joints [45]. Thus, in the present work, the thickness of reaction layers about 5-8μm obtained at 1183 and 1213 K for 1200 s are the optimum value.

Fig. 7 shows the morphology of the fracture surface of the TiAl/ZS joint brazed at 1183 K for 1200 s. From Fig. 7a, it can be concluded that, during the brazing process, the filler was well spread and the interface reaction is relatively full. No residual filler is observed in the fracture surface. Table 3 demonstrates the EDS results of fracture surface of brazed joint from Fig.7b. The compositions of fracture surface were mainly consisted of Zr and B elements. Thus, fracture occurred at the ZS side while the joint was unaffected. The strong joint feature was obtained under optimized parameters and in consistent with the results from Fig. 5.

Table 2 Chemical composition and possible phase of each spot marked in Figure 6 (at. %)

Position	Elements										Possible phase
	Ti	Zr	Cu	Ni	Al	B	Si	Nb	Cr	C	
O_1	26.91	15.07	39.00	8.87	1.38	3.81	0.71	1.04	0.76	2.44	residual filler
O_2	13.94	11.04	37.51	9.05	1.69	10.54	1.31	1.42	0.94	12.58	residual filler

Table 3 EDS results of fracture surface of brazed joint at 1183 K for 1200 s

Position	Elements							Phase
	Ti	Zr	Cu	Ni	Si	C	B	
1	0.02	15.64	0.13	0.19	2.15	-	81.87	ZS
2	0.36	12.03	1.09	1.01	1.93	-	83.59	ZS
3	0.56	15.12	0.75	0.49	2.01	-	81.97	ZS

Conclusion

In the present work, TiAl alloy and ZrB_2-SiC ceramic were tightly and strongly brazed with CuTiZrNi amorphous fillers. The reaction products of AlCuTi, Ti_2Al, $(Ti,Zr)_2(Cu,Ni)$, TiB,TiB_2, TiCu Ti_5Si_3, and TiC phase were detected in the brazed

joint. The mechanical properties testing results show that the shear strength is influenced by the brazing temperature which affects the thickness of reaction layers and brittleness of the intermetallic compounds in the joints. At 1183 K for 1200 s, an optimum thickness of reaction layers of 5-8 μm is achieved, leading to a maximum shear strength of 187 MPa. For other brazing temperature, either insufficient reaction or micro-crack takes place. As materials used in high temperature, TiAl/ZS are successfully brazed at an optimized temperature. Besides materials development, the present work is hoped to serve a promising route for future fabrications of high strength ceramics-metal complexes to be used under high temperatures.

Acknowledgement

This work was financially supported by the National Natural Science Foundation of China [51704001]; Natural Science Foundation of Anhui Province [KJ2018A0860, KJ2018A0113, KJ2018A0123, 1908085ME128]; Talent Project of Anhui Polytechnic University; and Talent Project of Anhui Province [Z175050020001]. W.C. acknowledges financial supports from the Academy of Finland [No. 311934] and the Anhui Provincial Grant for high-level platform construction.

References

1. Volker G, Melissa A, Joachim K, Helmut C. Metallurgical processing of titanium aluminides on industrial scale. Intermetallics 2018; 103: 12-22. https://doi.org/10.1016/j.intermet.2018.09.006
2. Wu XH. Review of alloy and process development of TiAl alloys. Intermetallics 2006; 14: 1114-1122. https://doi.org/10.1016/j.intermet.2005.10.019
3. Zghal S, Thomas M, Naka S, Finel A, Couret A. Phase transformations in TiAl based alloys. Acta Mater 2005; 53: 2653-2664. https://doi.org/10.1016/j.actamat.2005.02.025
4. Liu YY, Yao ZK, Guo HZ, Yang HH. Microstructure and property of the Ti-24Al-15Nb-1.5Mo/TC11 joint welded by electron beam welding. Int. J. Miner. Metall. Mater 2009; 16: 568-575. https://doi.org/10.1016/S1674-4799(09)60098-4
5. Lei ZL, Dong ZJ, Chen YB, Huang L, Zhu RC. Microstructure and mechanical properties of laser welded Ti–22Al–27Nb/TC4 dissimilar alloys. Mater Sci Eng A 2013; 559: 909-916. https://doi.org/10.1016/j.msea.2012.09.057
6. Du ZH, Zhang KF, Lu Z, Jiang SS. Microstructure and mechanical properties of vacuum diffusion bonding joints for γ-TiAl based alloy. Vacuum 2018; 150: 96-104. https://doi.org/10.1016/j.vacuum.2018.01.035
7. Simões S, Viana F, Kocak M, Ramos AS, Vieira MT, Vieira MF. Diffusion bonding of TiAl using reactive Ni/Al nanolayers and Ti and Ni foils. Mater Chem Phys 2011; 128: 202-207. https://doi.org/10.1016/j.matchemphys.2011.02.059
8. Simoes S, Ramos AS, Viana F, Vieira MT, Vieira MF. Joining of TiAl to steel by diffusion bonding with Ni/Ti reactive multilayers. Metals 2016; 6: 96. https://doi.org/10.3390/met6050096
9. Lee SJ, Wu SK. Infrared joining strength and interfacial microstructures of Ti-48Al-2Nb-2Cr intermetallics using Ti-15Cu-15Ni foil. Intermetallics 1999; 7: 11-21. https://doi.org/10.1016/S0966-9795(98)00004-1
10. Wang Y, Cai XQ, Yang ZW, Qiu QW, Wang DP, Liu YC. Microstructure evolution and mechanical properties of Ti-22Al-25Nb alloy joints brazed with Ti–Ni–Nb alloy. Mater Chem Phys 2016; 182: 488-497. https://doi.org/10.1016/j.matchemphys.2016.07.062
11. Shiue RK, Wu SK, Chen YT, Shiue CY. Infrared brazing of Ti50Al50 and Ti-6Al-4V using two Ti-based filler metals. Intermetallics 2008; 16: 1083-1089. https://doi.org/10.1016/j.intermet.2008.06.007
12. Dong D, Zhu DD, Wang Y, Wang G, Wu P, He Q. Microstructure and shear strength of brazing TiAl/Si_3N_4 joints with Ag-Cu binary alloy as filler metal. Metals 2018; 8: 896. https://doi.org/10.3390/met8110896
13. Zhao YX, Bian H, Fu W, Hu Y, Song XG, Liu D. Laser-induced metallization of porous Si_3N_4 ceramic and its brazing to TiAl alloy. J Am Ceram Soc 2019; 102(1): 32-36. https://doi.org/10.1111/jace.15937
14. Yang ZW, Lin JM, Wang Y, Wang DP. Characterization of microstructure and mechanical properties of Al_2O_3/TiAl joints vacuum-brazed with Ag-Cu-Ti+W composite filler. Vacuum 2017; 143: 294-302.

https://doi.org/10.1016/j.vacuum.2017.06.020
15. Dai XY, Cao J, Liu JQ, Wang D, Feng JC. Interfacial reaction behavior and mechanical characterization of ZrO_2/TC4 joint brazed by Ag-Cu filler metal. Mater Sci Eng A 2015; 646: 182-189. https://doi.org/10.1016/j.msea.2015.08.067
16. Li L, Li XQ, Hu K, He BL, Man H. Brazeability evaluation of Ti-Zr-Cu-Ni-Co-Mo filler for vacuum brazing TiAl-based alloy. T Nonferr Metal Soc 2019; 29(4): 754-763. https://doi.org/10.1016/S1003-6326(19)64985-X
17. Cao J, Song, XG, Li C, Zhao LY, Feng JC. Brazing ZrO_2 ceramic to Ti-6Al-4V alloy using NiCrSiB amorphous filler foil: Interfacial microstructure and joint properties. Mater Charact 2013; 81: 85-91. https://doi.org/10.1016/j.matchar.2013.04.009
18. Zhang XH, Hu P, Han JC. Structure evolution of ZrB_2-SiC during the oxidation in air. J Mater Res 2008; 23: 1961-1972. https://doi.org/10.1557/JMR.2008.0251
19. Qu ZL, He RJ, Cheng XM, Fang DN. Fabrication and characterization of B_4C-ZrB_2-SiC ceramics with simultaneously improved high temperature strength and oxidation resistance up to 1600^{o}C. Ceram Int 2016; 42: 8000-8004. https://doi.org/10.1016/j.ceramint.2016.01.202
20. Valenza F, Artini C, Passerone A, Muolo ML. ZrB_2-SiC/Ti6Al4V joints: wettability studies using Ag and Cu-based braze alloys. J Mater Sci 2012; 47: 8439–8449. https://doi.org/10.1007/s10853-012-6790-7
21. Valenza F, Artini C, Passerone A, Cirillo P, Muolo, ML. Joining of ZrB2 ceramics to Ti6Al4V by Ni-based interlayers. J Mater Eng Perform 2014; 23: 1555–1560. https://doi.org/10.1007/s11665-014-0868-0
22. Singh M, Asthana R. Joining and integration of ZrB_2-based ultra-high temperature ceramic composites using advanced brazing technology. J Mater Sci 2010; 45: 4308-20. https://doi.org/10.1007/s10853-010-4510-8
23. Yuan B, Zhang GJ. Microstructure and shear strength of self-joined ZrB_2 and ZrB_2–SiC with pure Ni. Scripta Mater 2011; 64: 17–20. https://doi.org/10.1016/j.scriptamat.2010.08.056
24. Liu YP, Wang G, Cao W, Xu HT, Huang ZJ, Zhu DD, Tan CW. Brazing ZrB_2-SiC ceramics to Ti6Al4V alloy with TiCu-based amorphous filler. J Manuf Processes 2017; 30: 516-522. https://doi.org/10.1016/j.jmapro.2017.10.021
25. Li ZR, Wang ZZ, Wu GD, Feng JC. Microstructure and mechanical properties of ZrB_2–SiC ultra high temperature ceramic composite joint using TiZrNiCu filler metal. Sci Technol Weld Join 2011; 16: 697-701. https://doi.org/10.1179/1362171811Y.0000000063
26. Wang G, Wang ZT, Wang W, He RJ, Gui KX, Tan CW, Cao W. Microstructure and shear strength of ZrB_2-SiC/Ti6Al4V joint by TiCuZrNi with Cu foam. Ceram Int 2019; 45: 10223-10229. https://doi.org/10.1016/j.ceramint.2019.02.074
27. Wang G, Wu P, Wang W, Zhu DD, Tan CW, Su YS, Shi XY, Cao W. Brazing Ti-48Al-2Nb-2Cr alloys with Cu-based amorphous alloy filler. Appl Sci 2018; 8: 920. https://doi.org/10.3390/app8060920
28. Wang G, Xiao P, Huang ZJ, He RJ. Brazing of ZrB_2-SiC ceramic with amorphous CuTiNiZr filler. Ceram Int 2016; 42: 5130-5135.

https://doi.org/10.1016/j.ceramint.2015.12.032
29. Liu XP, Zhang LX, Sun Z, Feng JC. Microstructure and mechanical properties of transparent alumina and TiAl alloy joints brazed using Ag-Cu-Ti filler metal. Vacuum 2018; 151: 80–89. https://doi.org/10.1016/j.vacuum.2018.01.019
30. Shiue RK, Wu SK, Chen SY. Infrared brazing of TiAl intermetallic using BAg-8 braze alloy. Acta Mater 2003; 51: 1991–2004. https://doi.org/10.1016/S1359-6454(02)00606-7
31. Yang SJ, Nam SW. Investigation of α_2/γ phase transformation mechanism under the interaction of dislocation with lamellar interface in primary creep of lamellar TiAl alloys. Mater Sci Eng A 2002; 329–331: 898–905. https://doi.org/ 10.1016/S0921-5093(01)01572-6
32. Cao GH, Skrotzki W, Gemming T. Transmission electron microscopy investigation of Ti_2Al precipitation in titanium aluminides during high-strain torsion. J Alloys Compd 2006; 417: 169–172. https://doi.org/ 10.1016/j.jallcom.2005.06.088
33. Xiong HP, Shen Q, Li JG, Zhang LM. Design and microstructures of Ti/TiAl/Al system functionally graded material. J Mater Sci Lett 2000; 19: 989–993. https://doi.org/ 10.1023/A:1006784709652
34. Li XQ, Li L, Hu K, Qu SG. Vacuum brazing of TiAl-based intermetallics with Ti–Zr–Cu–Ni–Co amorphous alloy as filler metal. Intermetallics 2015; 57: 7–16. https://doi.org/ 10.1016/j.intermet.2014.09.010
35. Li L, Li XQ, Hu K, Qu SG, Yang C, Li ZF. Effects of brazing temperature and testing temperature on the microstructure and shear strength of γ-TiAl joints. Mater Sci Eng A 2015; 634: 91-98. https://doi.org/ 10.1016/j.msea.2015.03.039
36. Lee JG, Choi YH, Lee JK, Lee GJ, Lee MK, Rhee CK. Low-temperature brazing of titanium by the application of a Zr–Ti–Ni–Cu–Be bulk metallic glass (BMG) alloy as a filler. Intermetallics 2010; 18: 70-73. https://doi.org/ 10.1016/j.intermet.2009.06.012
37. Cai YS, Liu RC, Zhu ZW, Cui YY, Yang R. Effect of brazing temperature and brazing time on the microstructure and tensile strength of TiAl-based alloy joints with Ti-Zr-Cu-Ni amorphous alloy as filler metal. Intermetallics 2017; 91: 35–44. https://doi.org/ 10.1016/j.intermet.2017.08.008
38. Herrmann D, Appel F. Diffusion bonding of γ-(TiAl) alloys: Influence of composition, microstructure, and mechanical properties. Metall Mater Trans A 2009; 40: 1881-1902. https://doi.org/ 10.1007/s11661-009-9878-1
39. Li XP, Wang HQ, Wang T, Zhang BG, Yua T, Li RS. Microstructural evolution mechanisms of Ti600 and Ni-25%Si joint brazed with Ti-Zr-Ni-Cu amorphous filler foil. J Mater Process Technol 2017; 240: 414-419. https://doi.org/ 10.1016/j.jmatprotec.2016.10.021
40. Wu MF, Yang M, Zhang C, Yang P. Research on the liquid phase spreading and microstructure of Ti/Cu eutectic reaction. Trans China Weld Inst 2005; 26(10): 68-71. https://doi.org/ 10.3321/j.issn:0253-360X.2005.10.018
41. Niu GB, Wang DP, Yang ZW, Wang Y. Microstructure and mechanical properties of Al_2O_3 ceramic and TiAl alloy joints brazed with Ag–Cu–Ti filler metal. Ceram

Int 2016; 42(6): 6924-6934. https://doi.org/ 10.1016/j.ceramint.2016.01.078
42. Wang G, Xiao P, Huang ZJ, He RJ. Brazing of ZrB_2-SiC ceramic with amorphous CuTiNiZr filler. Ceram Int 2016; 42: 5130-5135. https://doi.org/10.1016/j.ceramint.2015.12.032
43. Shiue RK, Wu SK, Chen YT. Strong bonding of infrared brazed α_2-Ti_3Al and Ti-6Al-4V using Ti-Cu-Ni fillers. Intermetallics 2010; 18: 107-114. https://doi.org/10.1016/j.intermet.2009.06.017
44. Wang G, Huang YJ, Wang GC, Shen J, Chen ZH. Brazing of Ti_2AlNb based alloy with amorphous Ti-Cu-Zr-Ni filler. J Wuhan Univ Technol 2015; 30: 617-621. https://doi.org/10.1007/s11595-015-1199-1
45. Wolfe DE, Jogender S, Krishnan N. Synthesis of titanium carbide/chromium carbide multilayers by the co-evaporation of multiple ingots by electron beam physical vapor deposition. Surf Coat Tech 2002; 160: 206-218. https://doi.org/10.1016/s0257-8972(02)00404-8

Figure Captions

Figure 1 a) Interfacial microstructure and elemental distribution of TiAl/ZS brazed joint b)Ti, c)Al, d)Cu, e) Ni, f)Zr, g)B, h)C, i)Si at 1213 K for 1200 s

Figure 2 SEM images of typical TiAl/ZS brazed joint at 1213 K for 1200 s

Figure 3 X-ray diffraction (XRD) pattern of fractured surface of brazed joint at 1213 K for 1200 s

Figure 4 Microstructural evolution of TiAl/ZS brazed joint a) and b) the interaction between filler and base materials; c), d) and e) the phase formation in the joint

Figure 5 Shear strengths of the brazed joint as a function of brazing temperature

Figure 6 Microstructure of TiAl/ZS brazed joints with different brazing parameters: a), b), c) 1153 K, 1200 s; d), e), f) 1183 K, 1200 s; g), h), i) 1213 K, 1200 s and j), k), l) 1243 K, 1200 s

Figure 7 Morphology of fracture surface of brazed joint at 1183 K for 1200 s

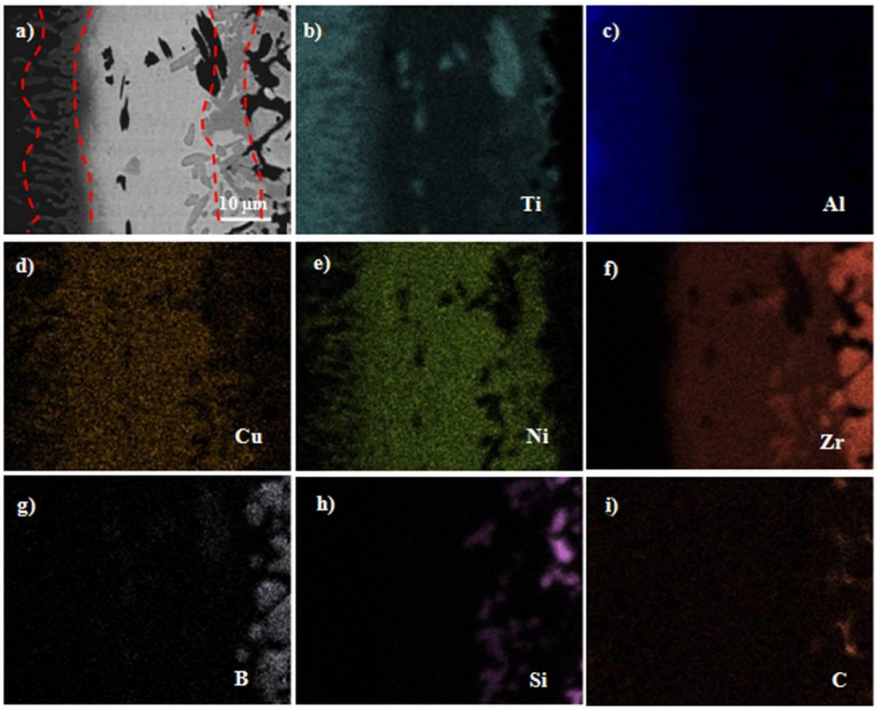
a)
10 μm
b)
Ti
c)
Al
d)
Cu
e)
Ni
f)
Zr
g)
B
h)
Si
i)
C

Fig.1

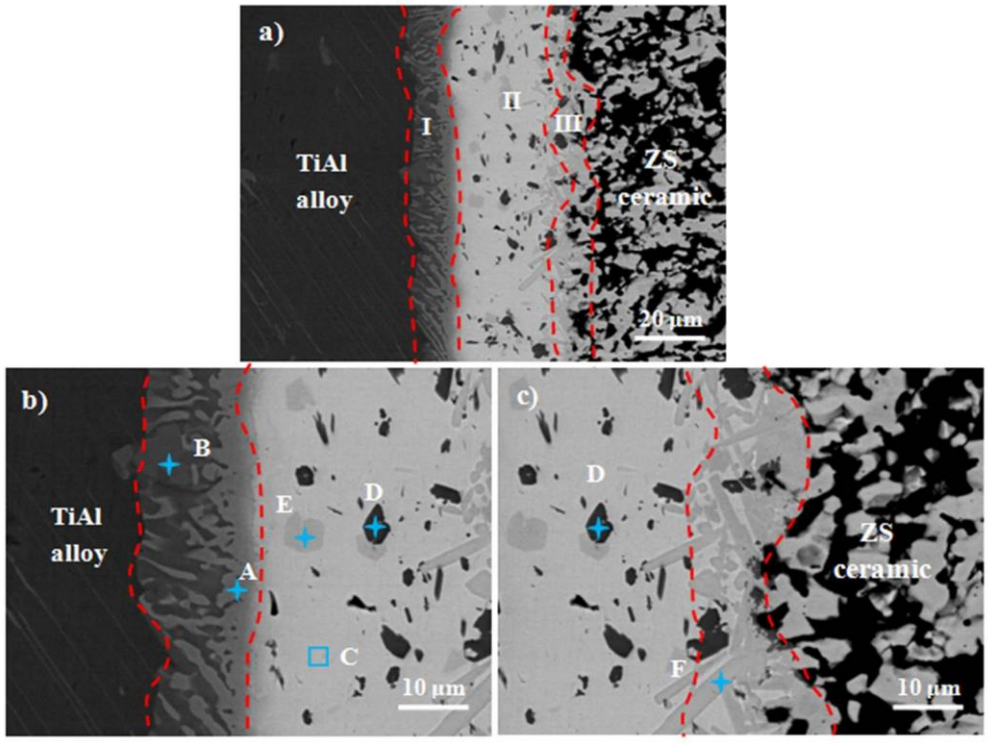
a)
TiAl
alloy
I
II
III
ZS
ceramic
20 μm
b)
TiAl
alloy
B
E
D
A
C
10 μm
c)
D
ZS
ceramic
F
10 μm

Fig.2

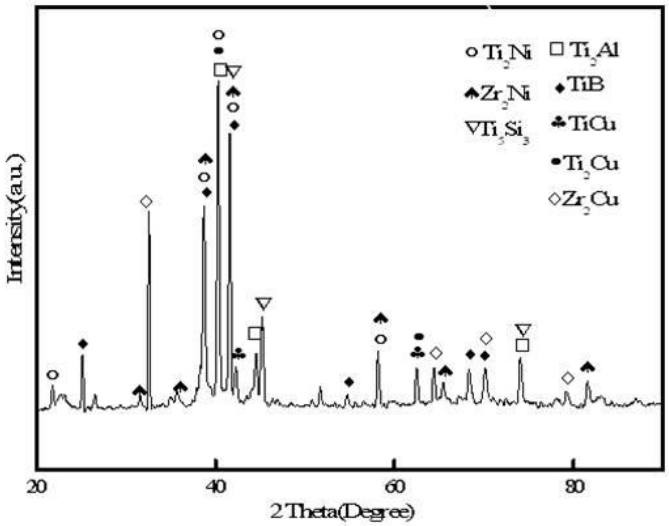

Fig.3

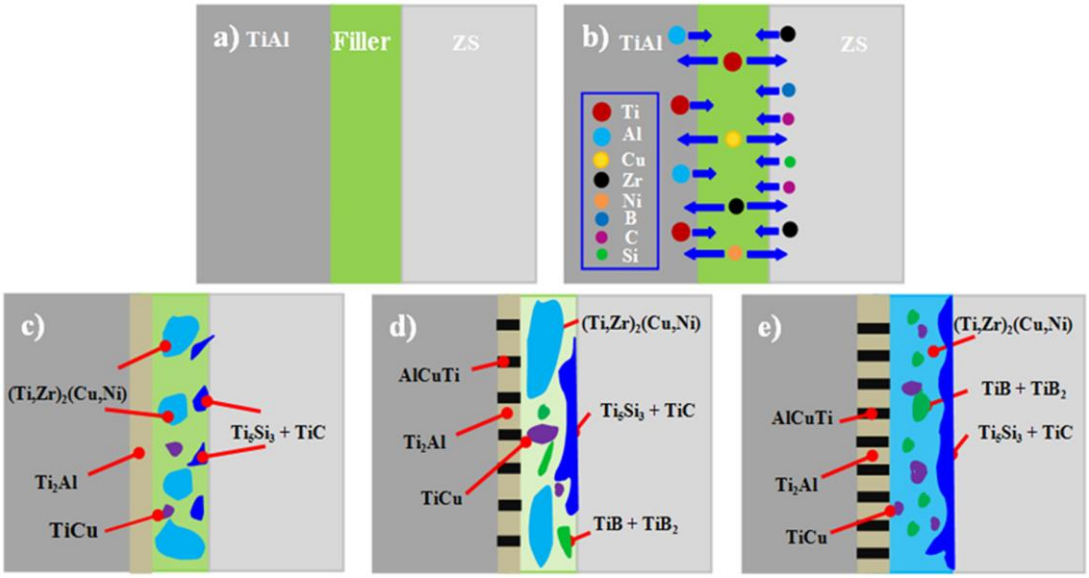

Fig.4

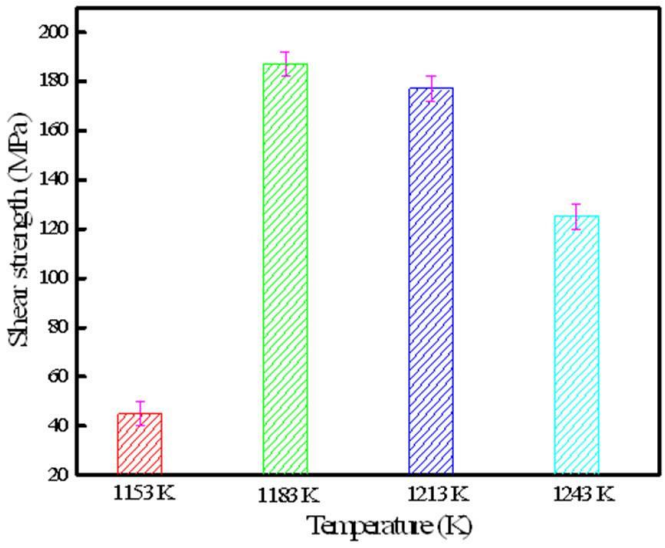

Fig.5

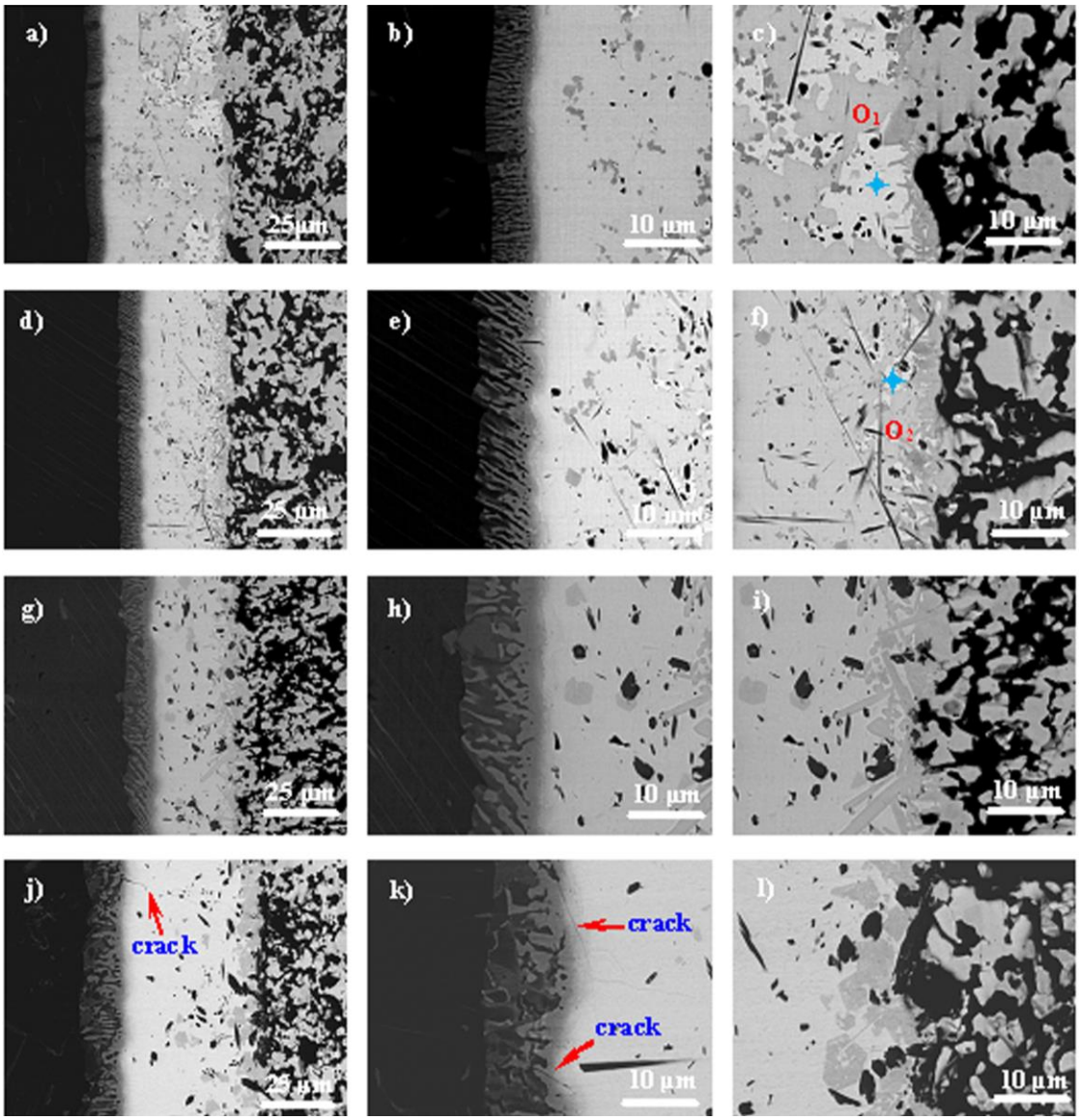
a)
25 μm
b)
10 μm
c)
O1
10 μm
d)
25 μm
e)
f)
O2
10 μm
g)
25 μm
h)
10 μm
i)
10 μm
j)
crack
k)
crack
crack
10 μm
l)
10 μm

Fig.6

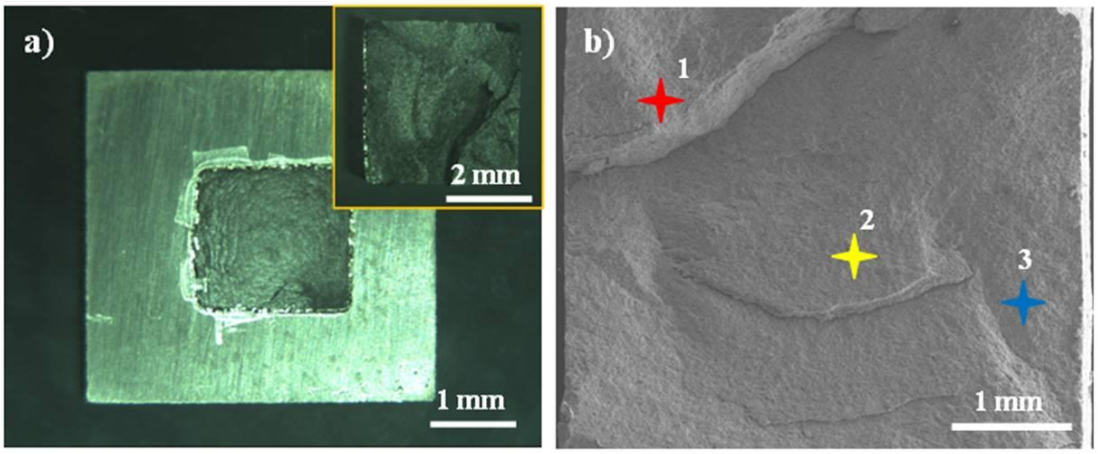
a)
2 mm
1 mm
b)
1
2
3
1 mm

Fig.7